GAMM-Mitt. **33**, No. 1, 8 – 24 (2010) / **DOI** 10.1002/gamm.201010002

Semismooth Newton methods for variational problems with inequality constraints

Corinna Hager[1,*] and **Barbara I. Wohlmuth**[2,**]

[1] Institut für Angewandte Analysis und Numerische Simulation, Universität Stuttgart
Pfaffenwaldring 57, 70569 Stuttgart, Germany
[2] Zentrum Mathematik der Technischen Universität München
Boltzmannstr. 3, 85748 Garching, Germany

Received 02 February 2010
Published online 27 April 2010

Key words Semismooth, Newton method, complementarity, inequality constraints
MSC (2000) 49M15, 65M60, 74C05, 74M10, 74M15, 76S05, 90C33, 90C53

Inequality constraints occur in many different fields of application, e.g., in structural mechanics, flow processes in porous media or mathematical finance. In this paper, we make use of the mathematical structure of these conditions in order to obtain an abstract computational framework for problems with inequality conditions. The constraints are enforced locally by means of Lagrange multipliers which are defined with respect to dual basis functions. The reformulation of the inequality conditions in terms of nonlinear complementarity functions leads to a system of semismooth nonlinear equations that is solved by a generalized version of Newton's method for semismooth problems. By this, both nonlinearities in the pde model and inequality constraints are treated within a single Newton iteration which converges locally superlinear. The scheme can efficiently be implemented in terms of an active set strategy with local static condensation of the non-essential variables. Numerical examples from different fields of application illustrate the generality and the robustness of the method.

1 Introduction

In many different applications, a system of partial differential equations needs to be solved subject to some inequality constraints. Three examples for such a situation are considered in this work, starting with a flow process in heterogeneous porous media where the local pressures of the phases need to excess a certain threshold in order to penetrate into the medium with smaller permeability. The second example, belonging to the field of mathematical finance, is to determine the fair price of an American option whose value cannot be lower than the payoff gained by exercising the option. Finally, we look at a setting from structural mechanics, namely the simulation of dynamic frictional contact of several elastoplastic bodies. The last example includes several inequality constraints describing the non-penetration of the bodies, the friction law as well as the plastification process inside the bulk media.

* Corresponding author E-mail: hager@ians.uni-stuttgart.de, Phone: +00 49 711 68565543
** E-mail: wohlmuth@ma.tum.de

All of the above sketched problems have been studied on their own; we refer to [1–5] and the references therein for an overview of the modeling of two-phase flow in heterogeneous porous media as well as to [6–10] and the corresponding references for the pricing of American options. An introduction to contact problems can be found in [11–14] and the references therein, while plastic effects have been analysed in [15–18] and the works cited therein.

In spite of the fact that the background of these applications is quite different, their common feature is the need to enforce inequality constraints on some part of the solution. Due to this, the weak form of these problems are variational inequalities [19–21] rather than variational equations. A common approach to treat these inequalities is to introduce additional dual variables beside the given primal ones and to formulate the constraints as a set of complementarity conditions [15, 22, 23]. There exist many different approaches to treat these nonlinear complimentarity constraints, e.g., interior point methods [24], SQP algorithms [23, 25], radial return mapping or cutting plane methods [18], as well as penalty or augmented Lagrangian approaches [13, 26]. For an overview of most of these methods, we refer to [27]. Another approach is to rewrite the inequality constraints as a set of nondifferentiable equations, termed nonlinear complementarity functions (see [19, 28–30] for some examples). Due to the lack of differentiability, the assumptions for the use of classical Newton methods [31] are not satisfied, but the so-called semismooth Newton method [19, 29, 32] can be applied.

In this paper, we employ the latter approach and reformulate the complimentarity conditions as a set of semismooth equations. Combined with the equilibrium equations describing the physical/financial process, a system of nonlinear semismooth equations is obtained that is solved in terms of a semismooth Newton method. The solution of the arising discrete tangential system is facilitated by choosing dual basis functions for the multipliers [33]. As a consequence, the complementarity conditions can be enforced locally and the semi-smooth Newton method can be interpreted as a primal-dual active set strategy [32, 34]. The use of active sets allows for local static condensation of either the additional inner/dual variables or the corresponding primal degrees of freedom, such that only a system of the size of the primal variable has to be solved in each Newton step. The generality of this approach can be seen by our various numerical examples for the three different fields of application.

The work is structured as follows: Section 2 presents the general equations for each of the three problems, as well as their discretization with respect to time and space. In Section 3, the resulting complementarity conditions are reformulated as sets of nondifferentiable equalities which can be solved by means of the primal-dual active set strategy described in Section 4. Section 5 contains numerical examples illustrating the generality and the robustness of this approach. The paper is concluded in Section 6.

2 Examples for problems with inequality constraints

In the following, we state the general equations for the three different applications and describe the physical/financial interpretation of the inequality constraints. Each problem is discretized in time by a suitable finite difference scheme, whereas the spatial discretization is adapted to the characteristics of the problem. Finally, for each of the three settings, we arrive at a system of nonlinear algebraic equations which has to be solved subject to nodal complementarity conditions.

2.1 Porous media: Two-phase flow with entry pressure

As the first example, we consider an incompressible two-phase flow process in heterogeneous porous media [35]. Assuming that we have no source/sink term and no gravity, the mass balance for the wetting phase ($\alpha = w$) and the nonwetting phase ($\alpha = n$) within the body $\Omega \subset \mathbb{R}^d$, $d \in \{2, 3\}$, is given by

$$\Phi \frac{\partial S_\alpha}{\partial t} + \operatorname{div} \mathbf{v}_\alpha = 0, \quad \alpha \in \{w, n\}, \quad t \in (0, T], \quad x \in \Omega, \tag{1}$$

where S_α is the unknown saturation of the phase α, Φ is the porosity, and $\mathbf{v}_\alpha$ is the Darcy velocity obtained from

$$\mathbf{v}_\alpha = -\xi_\alpha(S_\alpha) K \nabla p_\alpha.$$

There, we have introduced the permeability tensor K, the unknown pressure p_α of the phase α, as well as the mobility $\xi_\alpha := \frac{k_{r\alpha}}{\mu_\alpha}$ with the relative permeability $k_{r\alpha}$ and the viscosity μ_α.

To close the system, we employ the relation $S_n + S_w = 1$ as well as an enhanced capillary pressure–saturation relation that includes a dynamic retardation term [5, 36]:

$$p_n - p_w = p_c(S_n) = p_c^{\text{stat}}(S_n) + \tau \frac{\partial S_n}{\partial t}. \tag{2}$$

In (2), we have used the dynamic retardation factor $\tau \geq 0$ and the static capillary pressure function p_c^{stat} that is assumed to be continuously differentiable, strictly increasing and $p_c^{\text{stat}}(S_n) \to p_c^{\text{entry}} \geq 0$ for $S_n \to 0$. With these relations, the balance equations (1) can be cast into the following so-called fractional flow formulation (see, e.g., [37])

$$\Phi \dot{S}_n + \operatorname{div} \underbrace{\left(f(S_n) \mathbf{v}_t - \bar{\xi}(S_n) K \nabla p_c(S_n) \right)}_{=: \mathbf{v}(S_n)} = 0, \qquad \operatorname{div} \mathbf{v}_t = 0. \tag{3}$$

In (3), $\dot{S}_n := \frac{\partial S_n}{\partial t}$ denotes the time derivative, $\mathbf{v}_t := \mathbf{v}_w + \mathbf{v}_n$ is the total velocity, and the functions f and $\bar{\xi}$ are given by $f = \frac{\xi_n}{\xi_n + \xi_w}$ and $\bar{\xi} = \xi_w f$, respectively. The partial differential equation (3) has to be completed with suitable initial conditions for $t = 0$ and boundary conditions on $\partial\Omega$.

Next, we describe how the heterogeneity of the material is accounted for. For simplicity, we assume that the domain Ω is split into two subdomains Ω^m, Ω^s with the common interface Γ such that the parameters Φ and K are constant on each subdomain. Further, the domains are chosen such that the master subdomain Ω^m has a lower entry pressure $p_c^{m,\text{entry}}$ than the slave domain Ω^s, i.e., $p_c^{s,\text{entry}} \geq p_c^{m,\text{entry}}$.

Due to the jump in the material parameters, we need additional relations to describe the behavior of the flow at the interface Γ. Here, we restrict ourselves to the (physically more interesting) case that the nonwetting phase is penetrating from the subdomain with higher permeability to the one with higher entry pressure, i.e., from master to slave side; for the numerical treatment of the reverse case, we refer to [35] and Remark 4.1. As derived in [38], the pressure p_α is only continuous along Γ if the phase α is present on both sides. Thus, introducing the jump $[p_c] := p_c^s - p_c^m$ of the capillary pressure at the interface, we have to solve (3) on each of the subdomains Ω^m, Ω^s, subject to the following transmission conditions:

$$[p_c] \geq 0, \quad S_n^s \geq 0, \quad [p_c] S_n^s = 0. \tag{4}$$

In order to solve the above problem numerically, we first discretize (3) in time using equidistant time steps $t^i := i\Delta t$ and the implicit Euler method. For the spatial discretization, we apply a node-centered finite volume scheme [39] by introducing a shape-regular triangulation $\mathcal{T}_h^r$ of the subdomain Ω^r, $r \in \{s, m\}$, into simplices or quadrilaterals/hexahedrals and the corresponding dual mesh $\mathcal{T}_h^{*,r}$ (see [35, 39] for details). We remark that the meshes do not need to be matching at the interface Γ. Let $\mathcal{N}_h^r$, $r \in \{m, s\}$, denote the set of all nodes of $\mathcal{T}_h^r$ and let ϕ_j^r, $j \in \mathcal{N}_h^r$, be the corresponding conforming first order finite element basis functions, spanning the discrete space $V_h^r \subset H^1(\Omega^r)$. The saturation S_n is then approximated by $S_h = (S_h^s, S_h^m)$ with $S_h^r = \sum_{j\in\mathcal{N}_h^r} S_j^r \phi_j^r \in V_h^r$, $r \in \{m, s\}$. Further, let $\mathcal{C}_h$ be the set of slave nodes on Γ.

Integrating Equation (3) at time t^i on an element $T \in \mathcal{T}_h^{*,r}$ and using the divergence theorem, we obtain

$$\int_T \Phi \frac{S_h^i - S_h^{i-1}}{\Delta t}\, d\mathbf{x} + \int_{\partial T\setminus\Gamma} \mathbf{F}_{\text{num}}(S_h^i)\cdot \mathbf{n}_T\, ds + (-1)^{\delta_{rm}} \int_{\partial T\cap\Gamma} \lambda_h^i\, ds = 0, \quad (5)$$

with the unit outer normal $\mathbf{n}_T$ on ∂T, the Kronecker delta function δ_{rm} defined in (12), and the numerical flux $\mathbf{F}_{\text{num}}$ given by the following approximation of $\mathbf{v}$ on the boundary of T:

$$\mathbf{F}_{\text{num}}(S_h^i) := f(S_h^i)\mathbf{v}_t - \bar{\xi}(S_h^i)p_c'(S_h^i)K\nabla S_h^i.$$

The additional discrete variable $\lambda_h^i = \sum_{j\in\mathcal{C}_h} \lambda_j^i \psi_j^s \approx \mathbf{v}(S_h^i)\cdot\mathbf{n}_\Gamma$, with the unit normal $\mathbf{n}_\Gamma$ pointing into Ω^s, is introduced in order to enforce the interface conditions (4) and is defined as piecewise constant with respect to the dual mesh $\mathcal{T}_h^{*,s}|_\Gamma$. We refer to [40, 41] for an analysis of a related mixed discretization scheme.

The coefficient vectors of the discrete functions S_h^i, λ_h^i are denoted by $\mathbf{S}^i = (\mathbf{S}^{s,i}, \mathbf{S}^{m,i}) = \left(S_j^i\right)_{j\in\mathcal{N}_h}$ and $\boldsymbol{\lambda}^i = \left(\lambda_j^i\right)_{j\in\mathcal{C}_h}$, respectively. Summarizing Equation (5) for all $T \in \mathcal{T}_h^{*,r}$ on the subdomain Ω^r, $r \in \{s, m\}$, yields the nonlinear algebraic relation

$$\frac{1}{\Delta t} M_h^r \mathbf{S}^{r,i} + \mathbf{F}_h^r(\mathbf{S}^{r,i}) - G_h^r \boldsymbol{\lambda}^i = \frac{1}{\Delta t} M_h^r \mathbf{S}^{r,i-1}, \quad r \in \{s, m\}, \quad (6)$$

with the mass matrix M_h^r, the coupling matrix G_h^r and the nonlinear flux vector $\mathbf{F}_h^r(\mathbf{S}^{r,i})$.

In order to obtain a decoupled form of the complementarity conditions (4), we introduce the transfer matrix Π_h^s from master to slave side given by

$$(\Pi_h^s)_{jl} := \left(\int_\Gamma \psi_j^s\, ds\right)^{-1} \int_\Gamma \phi_l^m \psi_j^s\, ds, \quad j \in \mathcal{C}_h,\, l \in \mathcal{N}_h^m.$$

With this, we are able to construct the nodal version of (4) for $j \in \mathcal{C}_h$:

$$\begin{aligned} \left(p_c(S_j^{s,i}) - \left(\Pi_h^s p_c(\mathbf{S}^{m,i})\right)_j\right) \geq 0, \quad S_j^{s,i} \geq 0, \\ \left(p_c(S_j^{s,i}) - \left(\Pi_h^s p_c(\mathbf{S}^{m,i})\right)_j\right) S_j^{s,i} = 0. \end{aligned} \quad (7)$$

2.2 Mathematical finance: Basket American options

Next, we consider an application from the field of financial economics, namely European and American options. An European option is a contract which permits its owner to recieve a

certain payoff $\psi = \psi(\mathbf{x}) \geq 0$ at the expiry date T, depending on the value of the underlying assets $\mathbf{x}$ at time T. In contrast, an American option allows for obtaining the payoff ψ at any time τ between 0 and T. In this section, we consider options on a set of two assets $\mathbf{x} = (x_1, x_2)$. Employing some assumptions on the financial market like the no-arbitrage principle [8, 10], the fair price $P^{\text{eu}} = P^{\text{eu}}(\mathbf{x}, t)$ of an European put option satisfies the parabolic partial differential equation

$$\dot{P}^{\text{eu}} - \mathcal{L}P^{\text{eu}} = 0, \quad t \in (0, T], \quad \mathbf{x} \in \mathbb{R}^2_+, \tag{8}$$

with $t = T - \tau$ being the time to expiry, the operator

$$\mathcal{L} := \frac{1}{2} \sum_{k,l=1}^{2} \Xi_{k,l} x_k x_l \frac{\partial^2}{\partial x_k \partial x_l} + \sum_{k=1}^{2} (r - q_k) x_k \frac{\partial}{\partial x_k} - r, \tag{9}$$

the symmetric and positive definite volatility matrix

$$\Xi = \begin{pmatrix} \sigma_1^2 & \frac{2\varrho}{1+\varrho^2}\sigma_1\sigma_2 \\ \frac{2\varrho}{1+\varrho^2}\sigma_1\sigma_2 & \sigma_2^2 \end{pmatrix},$$

the correlation rate $\varrho \in [-1, 1]$, the fixed interest rate r and the dividend rates q_k on the asset x_k, $k \in \{1, 2\}$. Equation (8) is well-known as the Black–Scholes equation [7].

In case of an American option, the no-arbitrage principle implies that its fair value can never be below its payoff as the option can always be exercised. Further, a hedging argument yields that the Black–Scholes equation (8) becomes an inequality [8, 10]. Thus, the price P of an American put with payoff function ψ satisfies the following set of conditions for $\mathbf{x} \in \mathbb{R}^2_+$, $t \in (0, T]$:

$$\dot{P} - \mathcal{L}P \geq 0, \qquad P - \psi \geq 0, \qquad \left(\dot{P} - \mathcal{L}P\right)(P - \psi) = 0, \tag{10}$$

with the initial conditions $P|_{t=0} = \psi$. In order to enforce the first inequality constraint of (10), we introduce a Lagrange multiplier function $\lambda := \dot{P} - \mathcal{L}P$, leading to

$$\dot{P} - \mathcal{L}P - \lambda = 0, \qquad P - \psi \geq 0, \quad \lambda \geq 0, \quad \lambda\,(P - \psi) = 0. \tag{11}$$

To solve this problem numerically, we have to truncate the semi-infinite domain $\mathbb{R}^2_+$ to a finite block $\Omega := (0, \bar{x}_1) \times (0, \bar{x}_2)$ for some values of $\bar{\mathbf{x}}$ large enough. Next, the implicit second-order Crank–Nicolson scheme is used for time discretization, and the weak form of (11) is constructed via multiplication with a test function and integration over Ω. Appropriate Dirichlet boundary conditions P_D^i at time t^i, possibly depending on the choice of ψ, are enforced on the boundary of Ω (see [42] for details). Finally, we introduce a simplicial shape-regular triangulation $\mathcal{T}_h$ of Ω and approximate P^i on the space $V_h \subset H^1(\Omega)$ spanned by the lowest order conforming finite element basis functions ϕ_j, $j \in \mathcal{N}_h = \mathcal{J}_h \cup \mathcal{D}_h$, where $\mathcal{J}_h$ and $\mathcal{D}_h$ are the sets of all inner or boundary nodes of $\mathcal{T}_h$, respectively. The dual variable λ is approximated in $Q_h \subset L_2(\Omega)$ which is spanned by the basis functions ψ_j, $j \in \mathcal{J}_h$, satisfying the biorthogonality relation (see, e.g., [43])

$$(D_h)_{lj} := \int_\Gamma \phi_l^s \psi_j^s \, ds = \delta_{lj} \int_\Gamma \phi_j^s \, ds, \quad l, j \in \mathcal{J}_h, \quad \text{with } \delta_{lj} := \begin{cases} 1, & l = j, \\ 0, & \text{else.} \end{cases} \tag{12}$$

With this, we arrive at the discrete system for the inner degrees of freedom

$$\left(\frac{1}{\Delta t}M_h(\mathbf{P}^i-\mathbf{P}^{i-1})+\frac{1}{2}A_h(\mathbf{P}^i+\mathbf{P}^{i-1})\right)_{\mathcal{J}_h}-D_h\boldsymbol{\lambda}^i=0, \tag{13}$$

with M_h and A_h being the mass and the stiffness matrix associated with V_h, respectively, the latter steming from the weak form of the differential operator $\mathcal{L}$ (see [42] for details). Due to (12), the matrix D_h is diagonal and can thus easily be inverted.

Given $\mathbf{P}^{i-1}$, System (13) has to be solved for $(\mathbf{P},\boldsymbol{\lambda})^i$ together with the Dirichlet boundary conditions $\mathbf{P}^i_{\mathcal{D}_h}=\mathbf{P}^i_D$ and the nodewise complementarity conditions

$$P^i_j-\psi^i_j\geq 0,\quad \lambda^i_j\geq 0,\quad \left(P^i_j-\psi^i_j\right)\cdot\lambda^i_j=0,\quad j\in\mathcal{J}_h. \tag{14}$$

2.3 Structural mechanics: Frictional contact of elastoplastic bodies

Our final example is the modelling of frictional contact between several elastoplastic bodies [44]. As we will see in the following, this application includes several pairs of complementarity conditions, one in the inner of the domains describing the plastification process, and two sets on the boundary of the bodies for the normal contact and the friction law.

We consider a body $\mathbf{x}\in\Omega\subset\mathbb{R}^d$, $d\in\{2,3\}$, consisting of an elastoplastic material that can be modeled by infinitesimal associative plasticity. The sufficiently smooth boundary $\partial\Omega$ with unit outer normal $\mathbf{n}$ is partitioned into three nonoverlapping parts Γ_D, Γ_N and Γ_C; the body is clamped on Γ_D, whereas the traction forces $\mathbf{t}$ act on Γ_N, and Γ_C denotes the potential contact boundary. For sake of clarity, we restrict the further presentation to the case of homogeneous Dirichlet boundary conditions on Γ_D, unilateral contact of Ω with a rigid obstacle Ω_{obs} as well as linear hardening and friction laws. We stress that the framework is much more general and can be extended to the contact of several elastoplastic bodies [45] as well as to nonlinear material or hardening laws [18].

Let $\mathbf{u}$ denote the displacement vector, $\boldsymbol{\sigma}$ the Cauchy stress, $\boldsymbol{\varepsilon}$ the linearized strain tensor and $\mathbf{l}$ a given volume load. The strong forms of the governing equations are

$$\begin{aligned}
\rho\ddot{\mathbf{u}}-\operatorname{div}\boldsymbol{\sigma}&=\mathbf{l}, && \text{on }\Omega, && \mathbf{u}=\mathbf{0}, && \text{on }\Gamma_D,\\
\boldsymbol{\sigma}&:=C^{\text{el}}\boldsymbol{\varepsilon}^{\text{el}}:=C^{\text{el}}(\boldsymbol{\varepsilon}(\mathbf{u})-\boldsymbol{\varepsilon}^{\text{pl}}), && \text{on }\Omega, && \boldsymbol{\sigma}\mathbf{n}=\mathbf{t}, && \text{on }\Gamma_N,\\
\boldsymbol{\varepsilon}(\mathbf{u})&:=\tfrac{1}{2}(\nabla\mathbf{u}+\nabla\mathbf{u}^T), \quad \operatorname{tr}\boldsymbol{\varepsilon}^{\text{pl}}=\mathbf{0}, && \text{on }\Omega, && -\boldsymbol{\sigma}\mathbf{n}=\boldsymbol{\zeta}, && \text{on }\Gamma_C,
\end{aligned} \tag{15}$$

for each time instant $t\in(0,T]$. The first term in (15) with the density ρ covers the contribution of inertia; further, C^{el} denotes the Hooke tensor which can be written either in terms of the Lamé parameters λ, μ or with respect to the elasticity module E and the Poisson ratio ν [17]. The strain $\boldsymbol{\varepsilon}=\boldsymbol{\varepsilon}(\mathbf{u})$ is additively decomposed into its elastic and plastic part $\boldsymbol{\varepsilon}=\boldsymbol{\varepsilon}^{\text{el}}+\boldsymbol{\varepsilon}^{\text{pl}}$. In addition, we define its deviatoric part $\operatorname{dev}\boldsymbol{\varepsilon}:=\boldsymbol{\varepsilon}-\frac{1}{d}(\operatorname{tr}\boldsymbol{\varepsilon})\,\mathrm{Id}$, where $\mathrm{Id}\in\mathbb{R}^{d\times d}$ denotes the identity matrix and $\operatorname{tr}\boldsymbol{\varepsilon}$ is the trace of $\boldsymbol{\varepsilon}$. The initial conditions are given by $\mathbf{u}|_{t=0}=\mathbf{u}^0$ and $\dot{\mathbf{u}}|_{t=0}=\mathbf{v}^0$ as well as $\boldsymbol{\varepsilon}^{\text{pl}}|_{t=0}=\mathbf{0}$. For further information about the derivation and physical background of the plasticity and contact equations, we refer to [16–18] and [11–13], respectively, as well as to the references therein.

The additional unknowns $\boldsymbol{\zeta}:\Gamma_C\times(0,T]\to\mathbb{R}^d$ and $\boldsymbol{\varepsilon}^{\text{pl}}:\Omega\times(0,T]\to\{A\in\mathbb{R}^{d\times d}:A^T=A,\operatorname{tr}A=0\}$ in (15) are assumed to satisfy the laws of frictional contact with Tresca

or Coulomb friction and plasticity with linear isotropic or kinematic hardening, respectively:

$$\begin{aligned} &\zeta_n := \boldsymbol{\zeta}\cdot\mathbf{n}, \\ &\boldsymbol{\zeta}_t := \boldsymbol{\zeta} - \zeta_n\mathbf{n}, \end{aligned} \qquad \boldsymbol{\eta} := \operatorname{dev}\boldsymbol{\sigma} - a_0^{-2}K\boldsymbol{\varepsilon}^{\mathrm{pl}}, \tag{16a}$$

$$\begin{aligned} Y^{\mathrm{co}}(\zeta_n) &:= g_t + \mathfrak{F}\zeta_n, \\ f^{\mathrm{co}}(\zeta_n,\boldsymbol{\zeta}_t) &:= \|\boldsymbol{\zeta}_t\| - Y^{\mathrm{co}}(\zeta_n), \end{aligned} \qquad \begin{aligned} Y^{\mathrm{pl}}(\alpha) &:= a_0^{-1}(\sigma_0 + H\alpha), \\ f^{\mathrm{pl}}(\alpha,\boldsymbol{\eta}) &:= \|\boldsymbol{\eta}\| - Y^{\mathrm{pl}}(\alpha), \end{aligned} \tag{16b}$$

$$\dot{\mathbf{u}}_t = \begin{cases} \gamma^{\mathrm{co}}\frac{\boldsymbol{\zeta}_t}{\|\boldsymbol{\zeta}_t\|}, & \|\boldsymbol{\zeta}_t\| > 0, \\ \mathbf{0}, & Y^{\mathrm{co}}(\zeta_n) > \|\boldsymbol{\zeta}_t\| = 0, \end{cases} \qquad \dot{\boldsymbol{\varepsilon}}^{\mathrm{pl}} = \begin{cases} \gamma^{\mathrm{pl}}\frac{\boldsymbol{\eta}}{\|\boldsymbol{\eta}\|}, & \|\boldsymbol{\eta}\| > 0, \\ \mathbf{0}, & \|\boldsymbol{\eta}\| = 0, \end{cases} \tag{16c}$$

$$\begin{aligned} \gamma^{\mathrm{co}} &\geq 0, \\ -f^{\mathrm{co}}(\zeta_n,\boldsymbol{\zeta}_t) &\geq 0, \\ \gamma^{\mathrm{co}} f^{\mathrm{co}}(\zeta_n,\boldsymbol{\zeta}_t) &= 0, \end{aligned} \qquad \begin{aligned} \gamma^{\mathrm{pl}} &\geq 0, \\ -f^{\mathrm{pl}}(\alpha,\boldsymbol{\eta}) &\geq 0, \\ \gamma^{\mathrm{pl}} f^{\mathrm{pl}}(\alpha,\boldsymbol{\eta}) &= 0, \end{aligned} \tag{16d}$$

$$\begin{aligned} \zeta_n &\geq 0, \\ g(\mathbf{u}) := g_n - u_n &\geq 0, \\ \zeta_n g(\mathbf{u}) &= 0, \end{aligned} \qquad \dot{\alpha} = a_0^{-1}\gamma^{\mathrm{pl}}. \tag{16e}$$

On the left side of (16), the contact laws are displayed, beginning with the split of $\boldsymbol{\zeta}$ into its normal part ζ_n and its tangential part $\boldsymbol{\zeta}_t$ in (16a). The friction law consists of the flow rule (16c) for the tangential velocity $\dot{\mathbf{u}}_t$ and the complementarity conditions (16d) with respect to the consistency parameter γ^{co} and the yield function f^{co}. The friction parameters satisfy $\mathfrak{F}, g_t \geq 0$; the case $\mathfrak{F} = 0$ corresponds to Tresca friction, whereas for $g_t = 0$, the Coulomb friction law is obtained. The normal contact is described by the left side of (16e), enforcing the non-penetration of Ω and the obstacle by means of the normal gap function $g(\mathbf{u})$ (see [34] for details).

Comparing these relations with the plasticity laws on the right side of (16), many parallels can be seen. The plastic strain $\boldsymbol{\varepsilon}^{\mathrm{pl}}$ and the relative deviatoric stress $\boldsymbol{\eta}$ fulfill a similar flow rule (16c). Furthermore, the yield function f^{pl} and the consistency parameter γ^{pl} satisfy the same complementarity conditions (16d) as f^{co} and γ^{co}. The definition of f^{pl} employs the hardening parameters $H, K \geq 0$, the equivalent plastic strain α and the yield stress $\sigma_0 > 0$. The constant scaling factor $a_0^2 := \frac{d}{d-1}$ is used in order to have a consistent notation for both the two- and three-dimensional case.

One of the main differences between the conditions for contact and plasticity is the evolution law (16e) which causes the plasticity law to be associative, in contrast to the complementarity conditions for the normal contact. Another important difference is the higher regularity of the plastic inner stresses compared to the contact boundary stresses.

The discrete version of the coupled problem (15), (16) is derived similar to the previous examples, starting with time discretization using an implicit Newmark time stepping scheme with the parameters $\gamma = \beta = \frac{1}{2}$ (see, e.g., [13]). For the spatial discretization, we introduce a shape-regular triangulation $\mathcal{T}_h$ of the domain Ω such that the Dirichlet boundary Γ_D is resolved and denote all vertices of $\mathcal{T}_h$ not belonging to Γ_D by the index set $\mathcal{J}_h$. The nodes lying on the potential contact boundary Γ_C are pooled in the set $\mathcal{C}_h \subset \mathcal{J}_h$.

As before, ϕ_j denotes the lowest order conforming nodal finite element basis function associated with the node $j \in \mathcal{J}_h$, spanning the finite dimensional space $\mathbf{V}_h$. The plastic inner variables $(\alpha, \boldsymbol{\varepsilon}^{\mathrm{pl}})$ are approximated by the discrete space $\mathbf{Q}_h^{\mathrm{pl}}$, spanned by the piecewise

constant indicator functions χ_T, $T \in \mathcal{T}_h$. This leads to the discrete inner variables

$$\alpha_h = \sum_{T\in\mathcal{T}_h} \chi_T \alpha_T, \quad \boldsymbol{\varepsilon}_h^{\mathrm{pl}} = \sum_{T\in\mathcal{T}_h} \chi_T \boldsymbol{\varepsilon}_T^{\mathrm{pl}}, \quad \operatorname{dev} \boldsymbol{\sigma}_h = 2\mu \sum_{T\in\mathcal{T}_h} \chi_T \operatorname{dev}\left(\overline{\boldsymbol{\varepsilon}(\mathbf{u}_h)}_T\right), \tag{17}$$

with $\overline{\boldsymbol{\varepsilon}(\mathbf{u}_h)}_T$ denoting the mean value of $\boldsymbol{\varepsilon}(\mathbf{u}_h)$ on T. Hence, we have one plastic degree of freedom per element, which is a special case of the widely used approach to associate the plastic variables with the Gauß integration points [18,23]. We refer to [15] for the convergence analysis of a similar discretization.

To obtain a finite dimensional approximation of the contact stresses, we introduce the discrete space $\mathbf{Q}_h^{\mathrm{co}}$ spanned by the dual basis functions ψ_j, $j \in \mathcal{C}_h$, and set $\boldsymbol{\zeta}_h = \sum_{j\in\mathcal{C}_h} \boldsymbol{\zeta}_j \psi_j$. As in the previous examples, these basis functions are defined such that a biorthogonality relation similar to (12) is satisfied [33,46]. With this, we obtain the following system of equations for the coefficient vectors of the corresponding discrete functions in $\mathbf{V}_h \times \mathbf{V}_h \times \mathbf{Q}_h^{\mathrm{pl}} \times \mathbf{Q}_h^{\mathrm{co}}$: Given $(\mathbf{u}, \mathbf{v}, (\alpha, \boldsymbol{\varepsilon}^{\mathrm{pl}}), \boldsymbol{\zeta})^{i-1}$, find $(\mathbf{u}, \mathbf{v}, (\alpha, \boldsymbol{\varepsilon}^{\mathrm{pl}}), \boldsymbol{\zeta})^{i}$ satisfying

$$A_h \mathbf{u}^i + B_h^{\mathrm{pl}} \boldsymbol{\varepsilon}^{\mathrm{pl},i} + B_h^{\mathrm{co}} \boldsymbol{\zeta}^i - \mathbf{f}_h^{i-1} = \mathbf{0}, \qquad \frac{\mathbf{v}^i + \mathbf{v}^{i-1}}{2} = \frac{\mathbf{u}^i - \mathbf{u}^{i-1}}{\Delta t}, \tag{18}$$

subject to the discrete nodal version of the complementarity conditions in (16d) and (16e). For the definition of the stiffness matrix A_h, the coupling matrices B_h^{pl}, B_h^{co} and the right hand side vector $\mathbf{f}_h^{i-1}$, we refer to [44].

3 Reformulation as equality constraints

Although the examples described in Section 2 are quite different in nature, they all have the same basic structure, namely, a time-dependent partial differential equation subject to some complementarity constraints which are enforced by means of additional dual variables. In the following, we will show that these inequality constraints can equivalently be reformulated as a nonsmooth equality. There are several possibilities to define such nonlinear complementarity (NCP) functions (see, e.g., [19] and the references therein). Here, we use the functions employed in [34, 42, 44] which can be written in terms of the nodal trial values

$$S_j^{\mathrm{tr},i} := S_j^{s,i} + c_S\big(\left(\Pi_h^s p_c(\mathbf{S}^{m,i})\right)_j - p_c(S_j^{s,i})\big) \tag{19a}$$

$$\lambda_j^{\mathrm{tr},i} := \lambda_j^i + c_o h_j^{-1}(\psi_j^i - P_j^i) \tag{19b}$$

$$\begin{aligned} \zeta_{j,n}^{\mathrm{tr},i} &:= \zeta_{j,n}^i + c_n h_j^{-1}(u_{j,n}^i - g_{j,n}^i), \\ \boldsymbol{\zeta}_{j,t}^{\mathrm{tr},i} &:= \boldsymbol{\zeta}_{j,t}^i + c_t h_j^{-1}\left(\mathbf{u}_{j,t}^i - \mathbf{u}_{j,t}^{i-1}\right), \quad \boldsymbol{\eta}_j^{\mathrm{tr},i} := \boldsymbol{\eta}_j^i + c_p\left(\boldsymbol{\varepsilon}_j^{\mathrm{pl},i} - \boldsymbol{\varepsilon}_j^{\mathrm{pl},i-1}\right). \end{aligned} \tag{19c}$$

for any positive constants $c_S, c_o, c_p, c_t, c_n > 0$ and the local meshsize h_j. Furthermore, we introduce the notation $(\cdot)_+ := \max(0, \cdot)$.

Lemma 3.1 *The complementarity conditions* (7)*,* (14) *are equivalent to the equations*

$$C_j^{pm}(S_j^{s,i}, \mathbf{S}^{m,i}) := S_j^{s,i} - \left(S_j^{tr,i}\right)_+ = 0, \quad j \in \mathcal{C}_h, \tag{20}$$

$$C_j^{ao}(P_j^i, \lambda_j^i) := \lambda_j^i - \left(\lambda_j^{tr,i}\right)_+ = 0, \quad j \in \mathcal{J}_h, \tag{21}$$

respectively. Further, the conditions (16d), (16e) *in their discrete nodal form can be rewritten as*

$$C_j^{pl}(\mathbf{u}^i,(\alpha_j^i,\boldsymbol{\varepsilon}_j^i)) := \begin{pmatrix} \left(\|\boldsymbol{\eta}_j^{tr,i}\| - Y^{pl}(\alpha_j^i)\right)_+ - c_p a_0 \left(\alpha_j^i - \alpha_j^{i-1}\right) \\ \boldsymbol{\eta}_j^i - \min\left(1, \frac{Y^{pl}(\alpha_j^i)}{\|\boldsymbol{\eta}_j^{tr,i}\|}\right) \boldsymbol{\eta}_j^{tr,i} \end{pmatrix}, \quad j \in \mathcal{T}_h, \tag{22a}$$

$$C_j^{co}(\mathbf{u}_j^i,\boldsymbol{\zeta}_j^i) := \begin{pmatrix} \zeta_{j,n}^i - \left(\zeta_{j,n}^{tr,i}\right)_+ \\ \boldsymbol{\zeta}_{j,t}^i - \min\left(1, \frac{Y^{co}(\zeta_{j,n}^{tr,i})}{\|\boldsymbol{\zeta}_{j,t}^{tr,i}\|}\right) \boldsymbol{\zeta}_{j,t}^{tr,i} \end{pmatrix} \quad j \in \mathcal{C}_h. \tag{22b}$$

Proof. The rather technical proof consists of verifying the equivalence of the formulations by distinguishing between the different cases, as for example shown in [28,29]. We omit the details. □

Combining Equations (20), (21), (22) with the Systems (6), (13), (18), respectively, we obtain a system of nonlinear and nondifferentiable equations for each of the problems considered in Section 2. However, the NCP functions are piecewise differentiable and thus in particular semismooth, such that a generalized variant of the Newton scheme for semismooth problems can be used. The procedure is basically the same as the standard Newton method in all regions where the function is differentiable; at the other points, the values of the partial derivatives are defined by extending one of the derivatives from the neighborhood of the point. For the exact definition of semismoothness, we refer to [19,29,32], a detailed overview of Newton methods for nonlinear problems is given in [31].

Remark 3.2 The additional scaling factor h_j^{-1} in (19) is introduced in order to equilibrate the variables with respect to the mesh size. Similarly, the different scaling with respect to the material parameters should be respected by the choice of the constants c_S, c_o, c_p, c_t, c_n.

Remark 3.3 The solutions of the semismooth equations (20) to (22) do not change if some of the equations are multiplied with a nonzero factor. However, the local derivatives of the Newton method are altered if this factor depends on the primal or dual variables. Especially for the NCP functions (22), a multiplication of Equations (22a) and (22b) with the factors

$$\begin{pmatrix} 1 & \mathbf{0} \\ \mathbf{0} & \max\left(Y^{\mathrm{pl}}(\alpha_j^i), \|\boldsymbol{\eta}_j^{\mathrm{tr},i}\|\right)^s \mathrm{Id} \end{pmatrix}, \quad \begin{pmatrix} 1 & \mathbf{0} \\ \mathbf{0} & \max\left(Y^{\mathrm{co}}(\zeta_{j,n}^{\mathrm{tr},i}), \|\boldsymbol{\zeta}_{j,t}^{\mathrm{tr},i}\|\right)^s \mathrm{Id} \end{pmatrix}, \tag{23}$$

for $s \in (0,1]$, respectively, can improve the robustness of the resulting Newton scheme. We refer to [44] for details.

4 General solution algorithm

In this section, we sketch how the semismooth Newton method applied to one of the NCP functions (20) to (22) can efficiently be implemented. For sake of clarity, we restrict ourselves to the conditions of frictional contact (22b); we remark that the conditions (20) and (21) can be handeled similar as the normal contact conditions $(22b)_1$, and the plasticity case (22a) can be treated like the friction law $(22b)_2$.

The evaluation of the $(\cdot)_+$-symbol and the min-function in (22b) implies the following partitions of the set of potential contact nodes $\mathcal{C}_h$ into so-called active and inactive sets:

$$\mathcal{A}_n^i := \left\{ j \in \mathcal{C}_h : \zeta_{j,n}^{\mathrm{tr},i} > 0 \right\}, \ \mathcal{I}_n^i := \mathcal{C}_h \backslash \mathcal{A}_n^i, \tag{24}$$
$$\mathcal{A}_t^i := \left\{ j \in \mathcal{C}_h : \|\boldsymbol{\zeta}_{j,t}^{\mathrm{tr},i}\| > Y^{\mathrm{co}}(\zeta_{j,n}^{\mathrm{tr},i}) \text{ or } \|\boldsymbol{\zeta}_{j,t}^{\mathrm{tr},i}\| = Y^{\mathrm{co}}(\zeta_{j,n}^{\mathrm{tr},i}) = 0 \right\}, \ \mathcal{I}_t^i := \mathcal{C}_h \backslash \mathcal{A}_t^i.$$

Here, the active set $\mathcal{A}_n^i$ contains all nodes which are in contact with the obstacle at time t^i, whereas the nodes in $\mathcal{I}_n^i$ are free in the normal direction. The partition $\mathcal{A}_t^i$, $\mathcal{I}_t^i$ distinguishes between slippy and sticky nodes in the tangential direction, respectively. We remark that the case $\|\boldsymbol{\zeta}_{j,t}^{\mathrm{tr},i}\| = Y^{\mathrm{co}}(\zeta_{j,n}^{\mathrm{tr},i}) = 0$ can only occur for a free node in a problem with Coulomb friction and is included in $\mathcal{A}_t^i$ to get the correct boundary condition (see [34] for details).

With these sets, the NCP function (22b) with the additional factor (23) can be computed to

$$(22b)_1 = \begin{cases} \zeta_{j,n}^i, & j \in \mathcal{I}_n^i, \\ c_n h_j^{-1}(g_{j,n}^i - u_{j,n}^i), & j \in \mathcal{A}_n^i, \end{cases}$$
$$(22b)_2 = \begin{cases} -(Y^{\mathrm{co}}(\zeta_{j,n}^{\mathrm{tr},i}))^s c_t h_j^{-1}(\mathbf{u}_{j,t}^i - \mathbf{u}_{j,t}^{i-1}), & j \in \mathcal{I}_t^i, \\ \|\boldsymbol{\zeta}_{j,t}^{\mathrm{tr},i}\|^s \boldsymbol{\zeta}_{j,t}^i - Y^{\mathrm{co}}(\zeta_{j,n}^{\mathrm{tr},i}) \|\boldsymbol{\zeta}_{j,t}^{\mathrm{tr},i}\|^{s-1} \boldsymbol{\zeta}_{j,t}^{\mathrm{tr},i}, & j \in \mathcal{A}_t^i. \end{cases}$$

The application of the semismooth Newton method to these equations yields a local equation for the Newton update $(\delta\mathbf{u}_j^i, \delta\boldsymbol{\zeta}_j^i)$ which can be resolved for either the primal or the dual variable; e.g., for $j \in \mathcal{I}_n^i$, we obtain the Neumann condition $\delta\zeta_{j,n}^i = -\zeta_{j,n}^i$, whereas for $j \in \mathcal{A}_n^i$, the Dirichlet value $\delta u_{j,n}^i = g_{j,n}^i - u_{j,n}^i$ is obtained. Similarly, we can resolve the Newton equation of $(22b)_2$ for $\delta\mathbf{u}_{j,t}^i$, $j \in \mathcal{I}_t^i$, and $\delta\boldsymbol{\zeta}_{j,t}^i$, $j \in \mathcal{A}_t^i$ (see [44] for details). Substituting the resulting equations into the tangential system for the global unknowns $(\delta\mathbf{u}^i, \delta\boldsymbol{\zeta}^i)$, only a system of the size of the primal variables $\mathbf{u}$ has to be solved in each Newton iteration, and the condensed variables can be computed afterwards in a post-process.

For completeness, we state also the (in)active sets for the other applications. For the porous media equation (20), we obtain

$$\mathcal{A}_S^i := \left\{ j \in \mathcal{C}_h : S_j^{\mathrm{tr},i} > 0 \right\}, \ \mathcal{I}_S^i := \mathcal{C}_h \backslash \mathcal{A}_S^i. \tag{25}$$

Remark 4.1 If also the penetration of the nonwetting phase from slave to master side is allowed, we have to include the nodes $j \in \mathcal{C}^h$ with $p_c(S_j^{s,i}) - p_c(\Pi_h^s \mathbf{S}^{m,i})_j > p_c^{s,\mathrm{entry}} - p_c^{m,\mathrm{entry}}$ into the set $\mathcal{A}_S^i$ in order to allow for a non-zero saturation on the master side. We refer to [35] for details.

The American option equation (21) yields the sets

$$\mathcal{A}_o^i := \left\{ j \in \mathcal{J}_h : \lambda_j^{\mathrm{tr},i} > 0 \right\}, \ \mathcal{I}_o^i := \mathcal{C}_h \backslash \mathcal{A}_o^i. \tag{26}$$

Here, we can use these sets to obtain a spatial approximation of the exercise region $\{\mathbf{x} \in \Omega : P(\mathbf{x}) = \psi(\mathbf{x})\}$ (the set of triangles with active nodes), the continuation region (the set of triangles with at least one node in $\mathcal{I}_o^i$) and the exercise boundary.

Finally, for the plasticity law, we obtain

$$\mathcal{A}_p^i := \left\{ j \in \mathcal{T}_h : \|\boldsymbol{\eta}_{j,t}^{\mathrm{tr},i}\| > Y^{\mathrm{pl}}(\alpha_j^{\mathrm{tr},i}) \right\}, \quad \mathcal{I}_p^i := \mathcal{T}_h \backslash \mathcal{A}_p^i, \tag{27}$$

with $\mathcal{A}_p^i$ containing all elements where new plastification occurs.

5 Numerical results

This section contains several numerical examples which have been computed using the active set structure defined in (24) to (27). All active sets are initialized with the final active sets of the previous time step and are updated in each Newton iteration.

5.1 Porous media: Two-phase flow with entry pressure

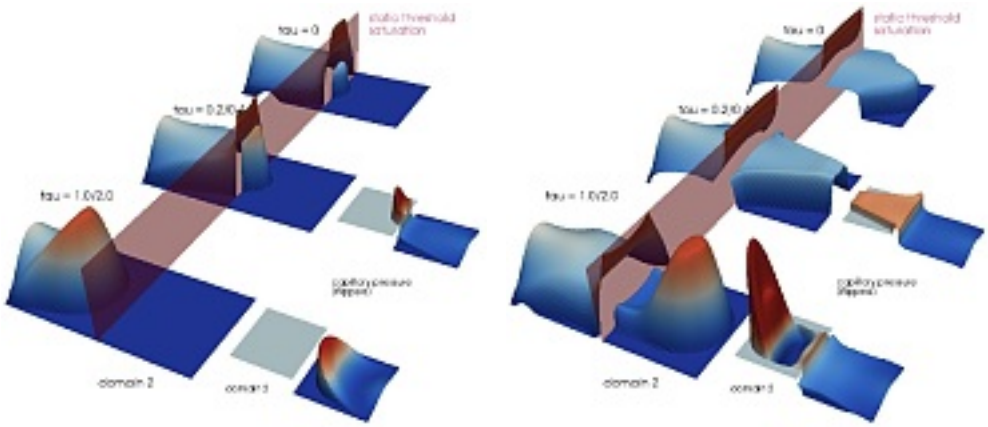

Fig. 1 (online colour at: www.gamm-mitteilungen.org) Porous media example 1: Saturation S_n and capillary pressure p_c for different values of τ^m, τ^s at time 0.5 (left) and 1 (right).

Our first numerical example uses two square domains Ω^m, Ω^s with the constant porosity $\Phi = 1$ but different permeabilities $K^m = \mathrm{Id}$, $K^s = \frac{1}{4}\,\mathrm{Id}$; the constitutive relationships are given by $p_c^{\mathrm{stat}}(S_n) = p_c^{\mathrm{entry}}(1 - S_n)^{-2}$ with $p_c^{s,\mathrm{entry}} = 4$, $p_c^{m,\mathrm{entry}} = 2$, and the relative permeability functions $k_{rw}(S_n) = (1 - S_n)^4$, $k_{rn}(S_n) = S_n^3(2 - S_n)$. The boundary conditions consist of Dirichlet values for S_n on the left side of Ω^m, outflow conditions on the right of Ω^s and no-flow conditions elsewhere. Initially, the whole domain is saturated with water, and the total velocity is given by $\mathbf{v}_t = (1, 0)^T$.

The saturation of the nonwetting phase as well as the capillary pressure for different values of the dynamic retardation parameter τ is shown in Figure 1. One can see the discontinuity in the saturations along the interface, with a penetration occuring after the capillary pressure has risen above the threshold in the entry pressures. Furthermore, the incorporation of τ allows for the formation of a shock front that cannot be modeled with the static capillary pressure.

The second example is a square domain Ω with four inclusions of lower permeability, as sketched on the upper left of Figure 2. We define the entry pressures on the subdomains by

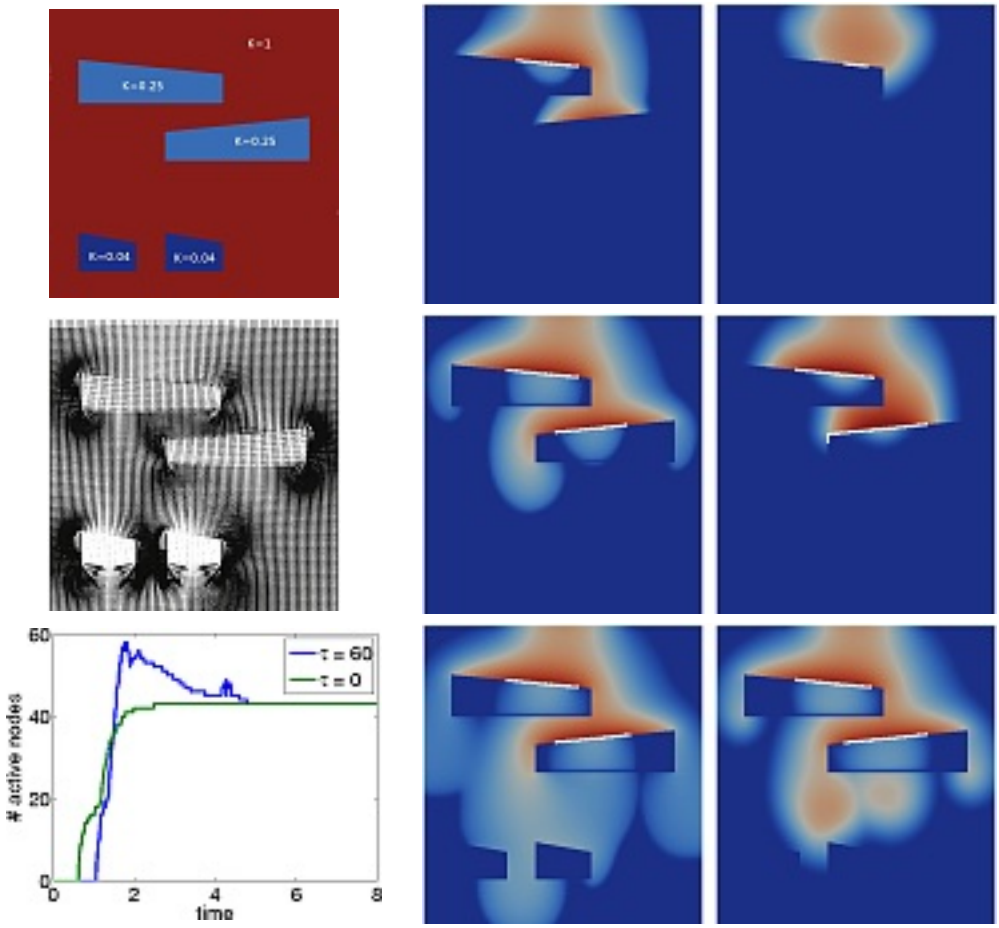

Fig. 2 (online colour at: www.gamm-mitteilungen.org) Porous media example 2: Left: Problem setting, fixed velocity field $\mathbf{v}_t$ and evolution of active set $|\mathcal{A}_S^i|$; middle and right: Saturation S_n for $\tau \in \{0, 60\}$ at times t_{110}, t_{200} and t_{350}.

$p_c^{\text{entry}} = 100K^{-1}$, use a quadratic relative permeability and apply the same initial conditions as before; further, we enforce an outflow boundary condition on the bottom of Ω and Dirichlet boundary conditions for S_n on the top. The time-independent velocity field $\mathbf{v}_t$ is shown on the left picture of the middle row of Figure 2. On the middle and the right of Figure 2, the saturation is shown for the dynamic parameters $\tau = 0$ and $\tau = 60$ after 110, 200 and 350 time steps with $\Delta t = 0.01$, respectively. The white marks illustrate the location of the active nodes where penetration occurs and the continuity of the capillary pressure is enforced. Finally, the lower left picture shows the evolution of the number of active nodes with respect to time. One can see that the upper two inclusions are penetrated by the nonwetting phase, in contrast to the lower ones whose entry pressure is never reached. Further, the inclusion of τ renders the solution more diffusive and changes the intermediate wave fronts as well as the size and the location of the active nodes. While the size of the active set is monotonically increasing for

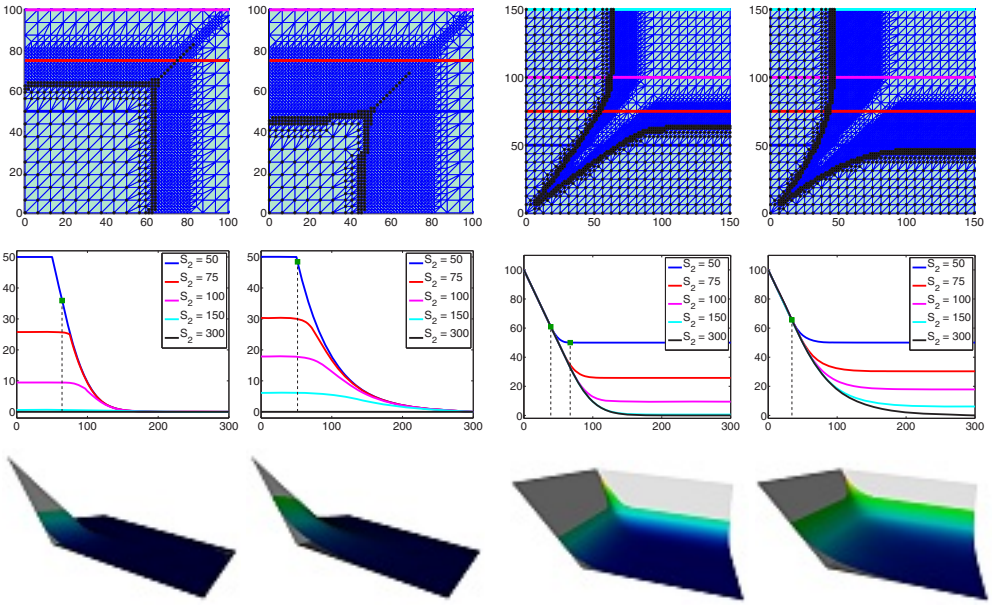

Fig. 3 (online colour at: www.gamm-mitteilungen.org) American option example: Meshes and solutions for payoff functions $\psi_{\max}$ (first and second row) and $\psi_{\min}$ (third and fourth row) at time steps t_5 and t_{20}.

$\tau = 0$, this is not the case for $\tau = 60$. This is because the additional dynamic term increases the capillary pressure for $\dot{S}_n > 0$, such that the entry pressure can be reached for smaller values of S_n. Thus, in the beginning of the simulation, the nonwetting phase has a wider area of penetration, as can be seen from the increase in the active set. However, as $\dot{S}_n$ tends to zero asymptotically, the value of τ does not influence the long-term behaviour of the system.

5.2 Mathematical finance: Basket American options

In this subsection, we present some numerical examples for the valuation of American options on the domain $\Omega := [0,\ 300]^2$ with one of the following two payoff functions [47]:

$$\psi_{\max}(\mathbf{x}) := (K - \max(x_1, x_2))_+ , \quad \psi_{\min}(\mathbf{x}) := (K - \min(x_1, x_2))_+ ,$$

where $K = 100$ is called the strike price. Further, we use the volatilities $\sigma_1 = \sigma_2 = 0.5$, the correlation ratio $\rho = 0.4$, the interest rate $r = 0.05$, the constant dividend factors $q_1 = q_2 = 0.015$ as well as the time step size $\Delta t = 0.05$. To be able to achieve more accurate results in the vicinity of the exercise boundary, we apply an adaptive mesh refinement strategy which refines the initial triangular grid near the boundary of the active region formed by the nodes in (26).

The upper row of Figure 3 shows a cutout of the meshes at the time steps t_5 and t_{20}, where the nodes marked in black belong to the active set (26). In the second row, the profiles of the solution $P_h(\mathbf{x})$ are displayed for several constant values of x_2 which are also indicated in the pictures of the first row. The intersections of the contour line for $S_2 = 50$ and the exercise

boundary are marked by the vertical dashed lines. The third row depicts three-dimensional plots of the option price $P_h(\mathbf{x})$ in combination with the obstacle.

5.3 Structural mechanics: Frictional contact of elastoplastic bodies

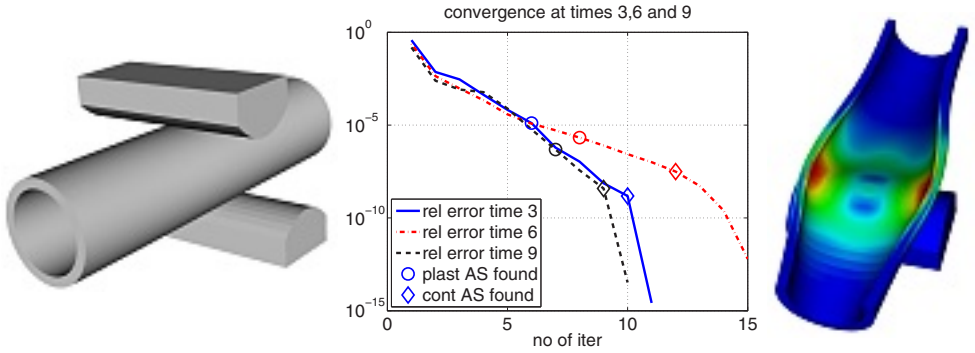

Fig. 4 (online colour at: www.gamm-mitteilungen.org) Plastic contact example: Geometry (left), convergence of Newton iteration at time steps t_3, t_6, t_9 (middle) and equivalent plastic strain α of upper half of the deformed tube at time t_9 (right).

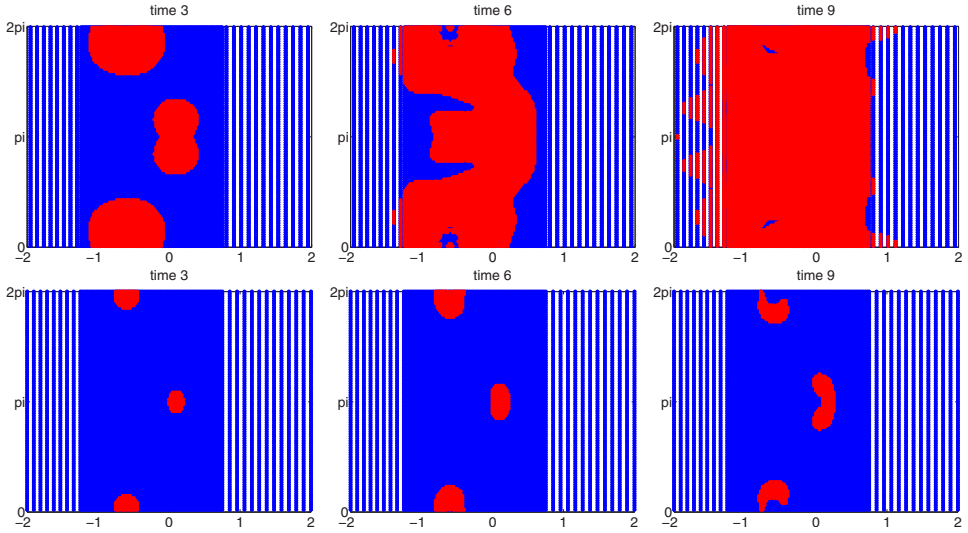

Fig. 5 (online colour at: www.gamm-mitteilungen.org) Plastic contact example: Position of active sets at time steps t_3, t_6, t_9; first row: plasticity; second row: contact.

Finally, we show a three-dimensional example for the frictional contact of several elastoplastic bodies. We consider a circular axisymmetric tube Ω^s which is squeezed by two curved tools Ω_1^m, Ω_2^m, as sketched on the left of Figure 4. The tube is fixed at one end and free otherwise, whereas the plates have a prescribed displacement of $\big(0, 0, -f_z(t)\big)$ on top of the

upper plate and $\big(0, 0, 2 \cdot f_z(t)\big)$ on the bottom of the lower plate, with $f_z(t) = f_z(t) = 800 \cdot \min(t, 2.5 \cdot 10^{-3} - t)$. The dynamic computation with hexahedral elements is performed in 21 time steps of step size $\Delta t = 2.5 \cdot 10^{-4}$; the material parameters are given by $E^m = 10^3 E^s = 7 \cdot 10^6$, $\nu = 0.3$, $\rho^m = 100\rho^s = 10^{-3}$, as well as $H = 2K = 2 \cdot 10^3$, $\sigma_0^m = 250\sigma_0^s = 5 \cdot 10^4$. In order to illustrate the generality of the method, we extend the linear isotropic hardening law considered in (16b) to the exponential law stated in [18] with $\sigma_\infty^m = 25\sigma_\infty^s = 10^5$, $k_e = 17$. We consider Coulomb friction with the friction coefficient $\mathfrak{F} = 0.1$; further, we use the additional factors for the NCP functions stated in Remark 3.3 with $s = 1$.

On the right of Figure 4, the computed equivalent plastic strain α after 9 time steps is depicted. The superlinear convergence of the quasi-Newton scheme can be seen in the middle picture, where the error decay at time steps 3, 6 and 9 is sketched. The symbols mark the Newton iteration where the correct plastic and contact active sets are found and not changed afterwards.

The evolution of these active sets is illustrated in Figure 5 depicting the position of the active nodes/elements at different time steps. The first row of pictures in Figure 5 shows the projection of the midpoint of each volume element onto a plane with respect to the x_1-value and the radial angle, the bottom side having the angle 0. Plastifying elements are marked with light color, whereas elements without new plastification give a darker mark. The second row displays the nodes on the potential contact surface, also with respect to the x_1-value and the angle. Inactive nodes are marked in dark and active (slippy) nodes in light colour. The axial symmetry of the problem formulation can easily be recognized in the numerical results.

6 Summary and conclusion

Inequality and complementarity constraints occur in many different applications; there exist many other examples besides those considered in this work. However, the mathematical structure of these conditions makes it possible to treat such problems within a general computational framework based on Lagrange multipliers with dual basis functions and semismooth Newton methods. One of the advantages of this approach is the consistent treatment of the constraints within the Newton iteration, thus avoiding nested loops for the material nonlinearity and the inequality constraints and still achieving local superlinear convergence. Furthermore, the nodal structure of the constraints allows for an easy static condensation of the additional dual degrees of freedom, such that the size of the tangential system is not increased. The numerical examples show that the resulting numerical scheme can efficiently solve even complex three-dimensional nonlinear systems.

Acknowledgements: We would like to thank Alexander Weiß and Dr. Stefan Hüeber for providing the numerical results for the porous media and American option examples.

References

[1] J. Bear, Dynamics of fluids in porous media (Dover Publications, Inc, New York, 1972).
[2] J. Bear and Y. Bachmat, Introduction to modelling of transport phenomena in porous media (Kluwer Academin Publishers, Dordrecht, 1991).
[3] C. J. van Duijn, J. Molenaar, and M. de Neef, Transport in Porous Media **21**, 71–93 (1995).

[4] R. Helmig, Multiphase flow and transport processes in the subsurface (Springer, 1997).
[5] S. Hassanizadeh and W. Gray, Water Resources Research **29**(10), 3389 – 3405 (1993).
[6] Y. Achdou and O. Pironneau, Computational methods for option pricing (SIAM, Philadelphia, 2005).
[7] F. Black and M. Scholes, J. Pol. Econ. **81**, 637–659 (1973).
[8] J. Hull, Options, futures, and other derivatives, 6 edition (Prentice Hall, 2006).
[9] P. Jaillet, D. Lamberton, and B. Lapeyre, Acta Appl. Math. **21**, 263–289 (1990).
[10] P. Wilmott, J. Dewynne, and S. Howison, Option pricing: Mathematical models and computation (Oxford Financial Press, Oxford, 1997).
[11] C. Eck, J. Jarušek, and M. Krbec, Unilateral contact problems. Variational methods and existence theorems (CRC Press Taylor & Francis Group, Boca Raton, 2005).
[12] N. Kikuchi and J. Oden, Contact problems in elasticity: A study of variational inequalities and finite element methods (SIAM Studies in Applied Mathematics 8, Philadelphia, 1988).
[13] T. Laursen, Computational contact and impact mechanics (Springer, Berlin Heidelberg, 2002).
[14] P. Wriggers, Computational contact mechanics (J. Wiley & Sons Ltd, Chichester, 2002).
[15] J. Alberty, C. Carstensen, and D. Zarrabi, Comput. Methods Appl. Mech. Engrg. **171**, 175–204 (1999).
[16] W. Han and B. D. Reddy, Comput. Mech. Advances **2**, 283–400 (1995).
[17] W. Han and B. D. Reddy, Plasticity - Mathematical theory and analysis (Springer, New York, 1999).
[18] J. C. Simo and T. J. R. Hughes, Computational inelasticity (Springer, Berlin Heidelberg, 1998).
[19] F. Facchinei and J. S. Pang, Finite-dimensional variational inequalities and complementary problems (Springer, New York, 2003).
[20] R. Glowinski, J. L. Lions, and R. Trémolières, Numerical analysis of variational inequalities (North-Holland, Amsterdam, 1981).
[21] D. Kinderlehrer and G. Stampacchia, An introduction to variational inequalities and their applications (SIAM, Philadelphia, 2000).
[22] W. Han, S. Jensen, and B. D. Reddy, Numer. Linear Alg. Appl. **4**(3), 191–204 (1997).
[23] C. Wieners, Z. Angew. Math. Mech. **87**(8), 643–660 (2007).
[24] S. J. Wright, Primal-dual interior point methods (SIAM, Philadelphia, 1997).
[25] J. S. Pang and S. A. Gabriel, Math. Progr. **60**, 295–337 (1993).
[26] R. Glowinski and P. Le Tallec, Augmented Lagrangian and operator splitting methods in nonlinear mechanics (SIAM Studies in Applied Mathematics 9, Philadelphia, 1989).
[27] C. Geiger and C. Kanzow, Theorie und Numerik restringierter Optimierungsaufgaben (Springer, Berlin Heidelberg, 2002).
[28] P. Alart and A. Curnier, Comput. Methods Appl. Mech. Engrg. **92**, 353–375 (1991).
[29] P. W. Christensen, Comput. Methods Appl. Mech. Engrg. **191**, 1189–1219 (2002).
[30] G. De Saxce and Z. Q. Feng, Mech. Struct. Mach. **19**, 301–325 (1991).
[31] P. Deuflhard, Newton methods for nonlinear problems – Affine invariance and adaptive algorithms (Springer, Berlin Heidelberg, 2004).
[32] M. Hintermüller, K. Ito, and K. Kunisch, SIAM J. Optim. **13**(3), 865–888 (2003).
[33] B. I. Wohlmuth, SIAM J. Numer. Anal. **38**, 989–1012 (2000).
[34] S. Hüeber, G. Stadler, and B. I. Wohlmuth, SIAM J. Sci. Comput. **30**(2), 572–596 (2008).
[35] R. Helmig, A. Weiss, and B. I. Wohlmuth, Comput. Geosci. **13**, 373–390 (2009).
[36] S. Hassanizadeh, M. Celia, and H. Dahle, Vadose Zone J. **1**, 38–57 (2002).
[37] P. Binning and M. A. Celia, Advances in Water Resources **22**(5), 461–478 (1999).
[38] M. de Neef, Modelling capillary effects in heterogeneous porous media, PhD thesis, University of Delft, Netherlands, 2000.
[39] R. Huber and R. Helmig, Comput. Geosci. **4**, 141–164 (2000).
[40] T. Arbogast, L. C. Cowsar, M. F. Wheeler, and I. Yotov, SIAM J. Numer. Anal. **37**(4), 1295–1315 (2000).

[41] T. Arbogast, G. Pencheva, M. F. Wheeler, and I. Yotov, Multiscale Model. Simul. **6**(1), 319–346 (2007).
[42] C. Hager, S. Hüeber, and B. I. Wohlmuth, Numerical techniques for the valuation of basket options and its greeks, Tech. Rep. 2008/012, Universität Stuttgart, IANS, 2008, to appear in J. Comput. Fin.
[43] B. I. Wohlmuth, Discretization Methods and Iterative Solvers Based on Domain Decomposition (Springer, 2001).
[44] C. Hager and B. I. Wohlmuth, Comput. Methods Appl. Mech. Engrg. **198**, 3411–3427 (2009).
[45] S. Hüeber and B. I. Wohlmuth, SIAM J. Numer. Anal. **43**(1), 157–173 (2005).
[46] B. Flemisch and B. I. Wohlmuth, Comput. Methods Appl. Mech. Engrg. **196**, 1589–1602 (2007).
[47] Y. Achdou and O. Pironneau, Appl. Math. Finance **12**(3), 201–241 (2005).

